Bound Topological Edge State in the Continuum for All-Dielectric Photonic Crystals

Zhanyuan Zhang,[1,‡] Zhihao Lan,[2,‡] Yaozu Xie,[1] Menglin L.N. Chen,[3] Wei E.I. Sha,[4,*] and Yi Xu[1,5,†]

[1] *Department of Electronic Engineering, College of Information Science and Technology, Jinan University, Guangzhou 510632, China*

[2] *Department of Electronic and Electrical Engineering, University College London, Torrington Place, London WC1E 7JE, United Kingdom*

[3] *Department of Electrical and Electronic Engineering, The University of Hong Kong, Hong Kong*

[4] *State Key Laboratory of Modern Optical Instrumentation, College of Information Science and Electronic Engineering, Zhejiang University, Hangzhou 310027, China*

[5] *Advanced Institute of Photonics Technology, School of Information Engineering, and Guangdong Provincial Key Laboratory of Information Photonics Technology, Guangdong University of Technology, Guangzhou 51006, China*

(Received 20 April 2021; revised 2 November 2021; accepted 15 November 2021; published 15 December 2021)

The canonical way to sustain photonic topological edge states relies on the interface formed by topologically trivial and nontrivial photonic crystals that share a common band gap to prevent the coupling of edge states from the radiation continuum of free space. Herein, we report a scheme to achieve bound topological edge states in the continuum at the air edge of a single topologically nontrivial photonic crystal utilizing the physics of bound states in the continuum. These localized states, though existing in the continuum, exhibit topological features inherited from the nontrivial topology of bulk photonic bands, such as pseudospin-momentum locking unidirectional propagation. Microwave experiments are provided to further validate the theoretical predictions. Our work not only has practical importance but also opens an avenue where the nontrivial topology of bulk photonic bands could be exploited to enrich the physics of bound states in the continuum.

DOI: 10.1103/PhysRevApplied.16.064036

I. INTRODUCTION

Topological insulators are electronic materials that are insulating in the bulk but host unusual conducting states on their surfaces due to the nontrivial bulk band topology [1]. Inspired by the development of topological insulators in condensed matter physics, topological photonics, which enables unidirectional electromagnetic wave propagation, has attracted growing attention recently [2,3]. In particular, different photonic systems have been explored to mimic the quantum Hall effect [4–10], quantum spin Hall (QSH) effect [11–21], and quantum valley Hall effect [22–28], and to realize three-dimensional photonic topological phases [29–31], Weyl point and Fermi arc [32,33], topological cavity [34], topological lasing [35–38], and defect modes [39,40]. According to the bulk-edge correspondence principle [1], gapless edge states will emerge within a frequency band gap of photonic systems with nontrivial bulk topology and exhibit interesting features for promising applications [2,3].

The generality of topological physics facilitates the photonic analogue of electronic systems [1–3]. However, there is a fundamental difference between topological electronic and photonic systems. In order to sustain topological edge states, two mediums forming the interface should have distinct topologies. In general, air is a trivial medium and it can serve as a hard boundary for electrons. However, light can propagate in air, resembling a radiation continuum for photons. Thus, the canonical way to form a topological photonic edge strictly relies on the interface between a trivial photonic crystal (PhC) and a nontrivial PhC sharing the common band gap [2,3]. However, in the microwave regime, one can create a confining edge by employing the interface formed by a PhC and a perfect electric conductor (PEC) to effectively eliminate the coupling between the edge state and the continuum [6], which cannot be generalized to the optical regime.

Being a counterintuitive localization mechanism of wave physics, bound states in the continuum (BICs) provide an exceptional way to confine waves in the radiation continuum [41–47]. Leveraged by state-of-the-art

*weisha@zju.edu.cn
†yi.xu@osamember.org
‡These authors contributed equally to this work.

nanofabrication technology, a PhC slab system supporting both symmetry-protected and accidental BICs becomes a promising platform for exploring fundamental physics [48–54] and functional applications [55–64]. In addition to the BICs of slab systems, there are also surface BICs in photonic systems [65–67]. In general, the topological edge state and BICs are physical mechanisms to confine electromagnetic fields in distinct frequency spectra, i.e., within the photonic band gap and radiation continuum, respectively.

In this article, we merge the physics of surface BICs and topologically nontrivial PhCs to introduce a concept of *bound topological edge states in the continuum*. We theoretically propose and experimentally demonstrate that topological edge states can be sustained within the radiation continuum empowered by BICs. Moreover, we show that such states inherit properties of canonical topological edge states at the interface between trivial and nontrivial PhCs, such as pseudospin-momentum locking unidirectional propagation of electromagnetic waves. While it has been revealed that BICs of photonic slabs are vortex centers of polarization directions in the far-field radiation carrying quantized topological charges [50], our work points to a different direction where the nontrivial topology of bulk photonic bands characterized by Berry curvature and Chern number can be exploited to enrich the physics of BICs.

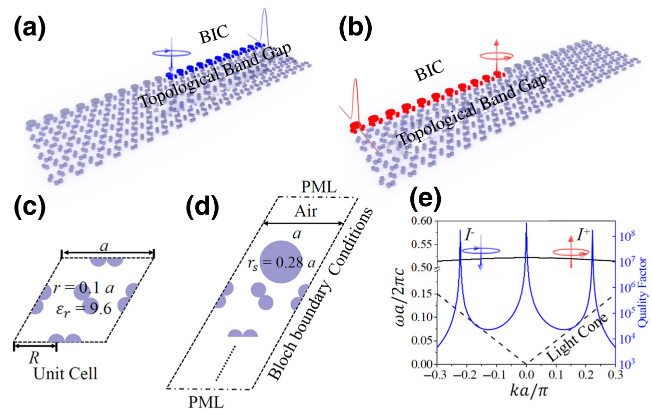

FIG. 1. (a),(b) Schematics of a PhC structure supporting bound topological edge states in the continuum enabled by topological band gap and BIC simultaneously. CPMD sources are used to excite unidirectional states propagating to the left and right, respectively. (c) The unit cell of the dielectric PhC hosting a topologically nontrivial band gap, which contains three pairs of attached pillars with $\varepsilon_r = 9.6$, $r = 0.1a$, and $R = 0.4a$. (d) The supercell of the PhC structure supporting the bound topological edge states in the continuum, where the PhC is truncated and defect pillars with a different radius r_s are introduced at the edge. (e) The calculated dispersion and corresponding Q factors of the edge mode above the light cone with $r_s = 0.28a$, where two modes with divergent Q factors (I^- and I^+) are the bound topological edge states in the continuum without any leakage to air.

II. CONCEPT AND MECHANISM

The key idea of our work is to demonstrate the existence of bound topological edge states in the continuum at the air edge of a topologically nontrivial PhC, where the edge states are guided by the BIC and topological band gap simultaneously. They can be selectively excited by circularly polarized magnetic dipole (CPMD) sources, as schematically shown in Figs. 1(a) and 1(b). The transverse magnetic mode of a two-dimensional PhC is considered. We consider a widely used scheme mimicking the QSH effect in a two-dimensional expanded honeycomb lattice of dielectric cylinders ($R = 0.35a$, $0.36a$, and $0.38a$) similar to the canonical all-dielectric topological PhC proposed by Wu and Hu [15], where the structures are shown in Fig. 2(a). Due to the C_{6v} symmetry of the system, there are two two-dimensional irreducible representations of the C_{6v} symmetry group, which are realized by the degenerate $p_x(p_y)$ and $d_{xy}(d_{x^2-y^2})$ orbits. Moreover, pseudospin-up and pseudospin-down states can be constructed as $p_\pm = (p_x \pm ip_y)/\sqrt{2}$, $d_\pm = (d_{x^2-y^2} \pm id_{xy})/\sqrt{2}$, where the role of pseudospin is indicated by the angular momentum of the wave function (the out-of-plane electric field in this case). By simply shrinking or expanding the six dielectric cylinders in the hexagonal unit cell towards or opposite the center, a topological trivial or nontrivial band gap can be opened around the doubly degenerate Dirac cone, which is accompanied by band inversion between the $p_x(p_y)$ and $d_{xy}(d_{x^2-y^2})$ orbits. It is confirmed that there are nontrivial photonic band gaps opened for these three cases ($R = 0.35a$, $0.36a$, and $0.38a$).

By truncating such a PhC [see Fig. 2(b)] with another triangular PhC that possesses a trivial band gap, two QSH edge defect bands are formed within the overlapping band gap, as can be seen in Fig. 2. We start from the topological edge states formed by interfacing the nontrivial PhC with a trivial dielectric PhC that consists of a triangle lattice [see the upper part of the structure in Fig. 2(b)]. Such a trivial PhC, which supports a trivial photonic band gap spectrally overlapping with the nontrivial band gap, is different from the one shown in Ref. [15]. As can be seen from Fig. 2(c), there are two topological edge defect bands within the band gap, where their dispersion features resemble the typical QSH effect in an all-dielectric PhC shown in Ref. [15].

If the period number of the trivial PhC is gradually reduced, most of the defect modes become leaky due to the reduced band-gap effect at the trivial side of the interface, as shown in Figs. 3(a)–3(e) for the case of $R = 0.38a$. While the upper band of the QSH edge modes becomes highly leaky, the lower band shows certain robustness against such leaky effect. Comparing the modes of the

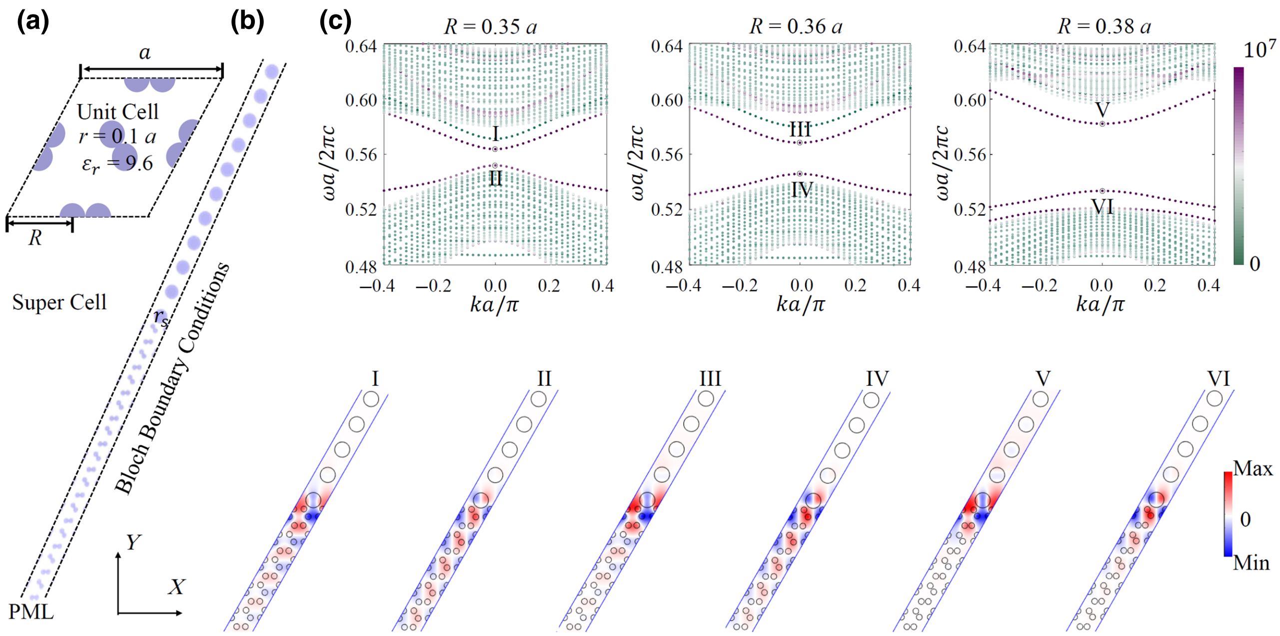

FIG. 2. The unit cell of the dielectric PhC emulating the QSH effect proposed in Ref. [15]. (b) The supercell of a domain-wall structure formed by interfacing the nontrivial PhC shown in (a) and a trivial PhC consisting of a single dielectric pillar in each unit cell with radius $r_s = 0.28a$. (c) The modal dispersion and the corresponding Q factors (color code) of eigenmodes for the structure shown in (b) with different expanded lattices at $R = 0.35a$, $R = 0.36a$, and $R = 0.38a$ (length of the hexagon edge). The corresponding distributions of electric field $\mathrm{Re}(E_z)$ for modes marked by I, II, III, IV, V, and VI are also provided.

upper and lower defect bands at $k = 0$ shown in Fig. 2 (I–VI), one can find that the eigenmodes of upper band at $k = 0$ (I, III, V) are even with respect to the Y axis while the eigenmodes of lower band at $k = 0$ (II, IV, VI) are odd with respect to the Y axis, which indicates that the coupling between the upper band and radiative continuum (free space) is more effective than the lower one. Therefore, the edge states of the upper band quickly change to highly leaky modes when the period of the trivial PhC is reduced. In sharp contrast, the Q factors of edge states at the lower band are still high regardless of the reduction of the trivial PhC's number of periods. Especially, all modes of the lower QSH band become highly leaky modes except for a symmetry-protected BIC at $k = 0$ when only one period of the trivial PhC is left, as shown in Figs. 1(e) and 3(e). More importantly, two accidental BICs can also be formed at certain k vectors [see Fig. 3(e) and (V) for example] of the band by fulfilling the destructive interference condition [67]. The distributions of electric field $\mathrm{Re}(E_z)$ and Poynting vectors for the accidental BIC in Fig. 3 (V) are similar to the case of the canonical topological edge state shown in Fig. 3 (I). Both the similarity of band dispersion and vectorial field distribution with features of pseudospin-momentum locking indicate that the bound topological edge state in the continuum is evolved from the topological edge state shown in Fig. 3(a) and the proposed bound topological edge state in the continuum could inherit the nontrivial topology of bulk photonic bands.

III. NUMERICAL RESULTS

Based on this general mechanism to form such topological BICs and for the convenience of experimental observations, in the following we consider the case when the expanding cylinders form attached dimers, as shown in Fig. 1(c). Defect cylinders with radius r_s are introduced at the boundary [see Fig. 1(d)], which serve as a "knob" to tune the properties of the emerging bound edge states. The calculated dispersion of the edge modes within the topological band gap is shown in Fig. 1(e) (see Fig. S1 within the Supplemental Material for the whole band structures [68]). As can be seen from this figure, the edge states exist above the light cone, i.e., within the radiation continuum of free space. The corresponding quality (Q) factors of these edge states are also shown in Fig. 1(e), from which we can clearly identify three modes whose Q factors are divergent, i.e., they are perfectly bound at the edge without any leakage to the air and the PhC. Of the three modes, the one at $ka/\pi = 0$ is a symmetry-protected BIC while the other two marked by I^- (pseudospin down) and I^+ (pseudospin up) are accidental BICs with inherent helicity. The

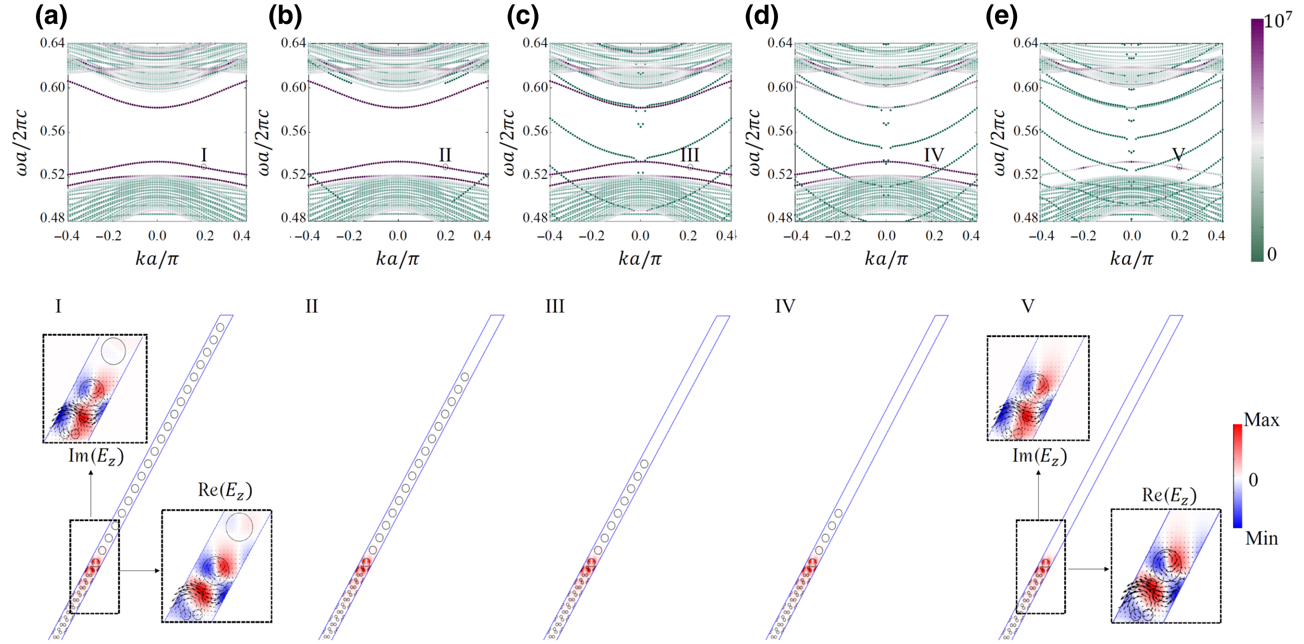

FIG. 3. The dependence of modal dispersion and Q factors (color code) on the number of pillars in the trivial PhC region. Here, 20 (a), 16 (b), 9 (c), 5 (d), and 1 (e) pillars in the trivial PhC region are considered. Here, $R = 0.38a$ and the pillars' radius of the trivial PhC is $r_s = 0.28a$ (a is the period of the lattice). The corresponding distributions of electric field $\mathrm{Re}(E_z)$ for modes marked by I, II, III, IV, and V are provided. The distributions of Poynting vectors for I and V are also presented.

field profiles of these bound topological edge states decay exponentially into both the free space and the PhC (see Fig. S2 within the Supplemental Material for the corresponding field profiles [68]).

Figure 4(a) shows the phase distributions of E_z for two edge states marked by I^- and I^+ in Fig. 1(e), where phase vortex centers can be clearly identified within both the boundary cylinder and the region enclosed by the three pairs of attached cylinders. Moreover, the phase winding directions of I^- and I^+ are opposite to each other. Figure 4(b) further shows the real parts of E_z and the time-averaged Poynting vectors (arrows) of I^- and I^+. Again, the Poynting vectors rotate clockwise (I^-) or anticlockwise (I^+) around the phase vortex centers shown in Fig. 4(a). Meanwhile, the electromagnetic energy flows from one supercell to its neighbor supercell, forming an effective wave-guiding channel. As these two states (I^- and I^+) have opposite momenta, the inherent helicity (i.e., pseudospin) manifested as the phase vortex centers and rotating Poynting vectors implies the

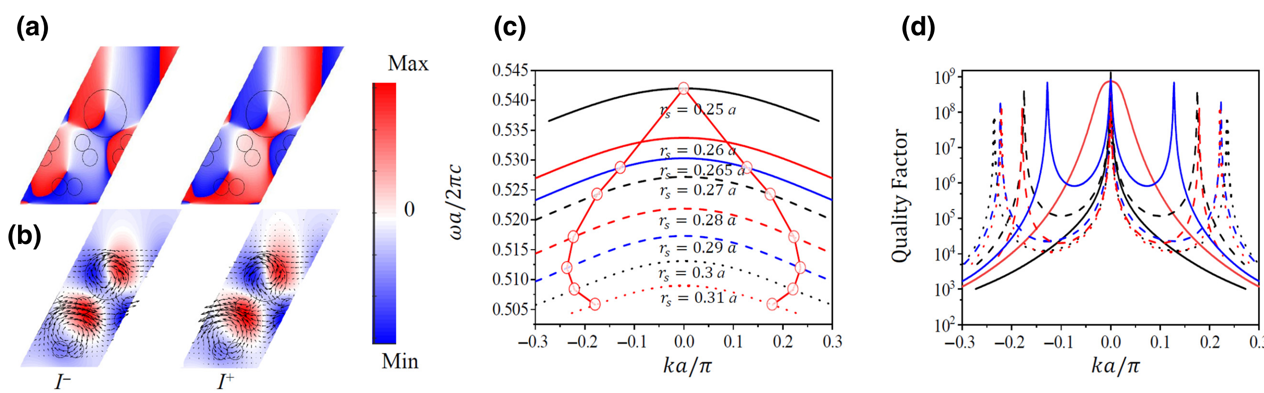

FIG. 4. (a) Phase distributions of E_z. (b) Real parts of E_z and Poynting vectors for two eigenmodes marked by I^- and I^+ in Fig. 1(e), from which the inherent helicity of the two modes can be clearly seen. (c) Evolution of the bound topological edge states in the continuum as a function of r_s, where a "heart"-shaped trajectory indicates the frequencies of the I^- and I^+ modes. (d) The corresponding Q factors for (c).

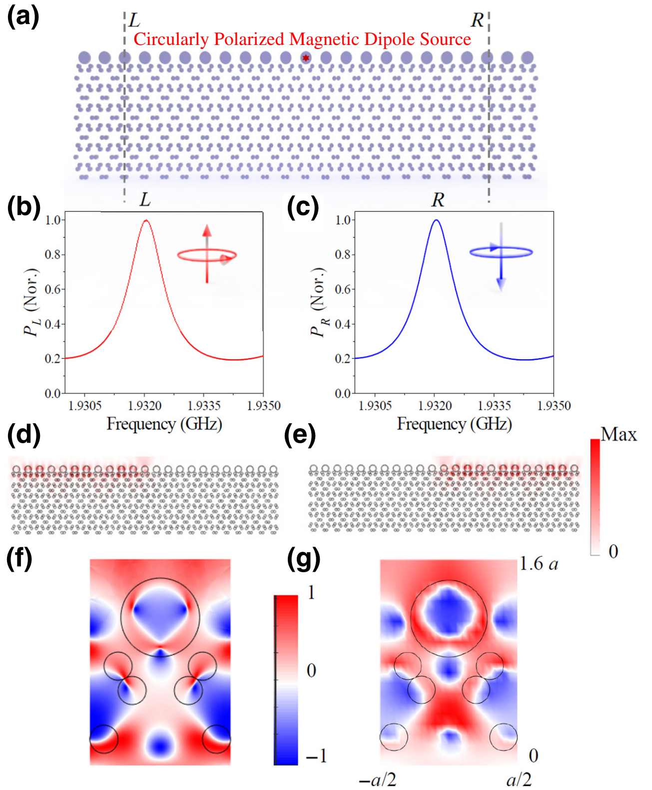

FIG. 5. (a) A finite structure of 23 periods supporting quasibound topological edge states in the continuum. The location of CPMD sources is marked by the star. (b),(c) Normalized powers along the left (L) and right (R) directions as a function of excitation frequency at $a = 80$ mm, which are obtained by integrating the powers along the dashed lines (L and R) marked in (a). (d),(e) Distributions of electric field amplitude ($|E_z|$) at the peaks in (b) and (c), respectively. (f) The Stokes parameter S_3 retrieved from the eigenmode of I^+. (g) Directionality $D(x, y)$ retrieved from full-wave simulations under the excitation of a pseudospin-up magnetic dipole source at a frequency of 1.9321 GHz.

pseudopsin-momentum locking behavior of the electromagnetic field propagation, a hallmark of the QSH effect. Furthermore, both the vectorial field distribution of the accidental BIC and the dispersion of the leaky band are similar to those of the corresponding QSH edge states (see Fig. 3), revealing an interesting correspondence between the bound topological edge states in the continuum and the canonical topological QSH edge states. The effects of defect size r_s on the dispersion and Q factors of edge modes are shown in Figs. 4(c) and 4(d), respectively. The trajectories of I^- and I^+ when changing r_s form a "heart" shape and they merge at $k = 0$ when $r_s = 0.25a$, where merging BICs in momentum space can be observed (see the case of $r_s = 0.26a$) [58].

The inherent helicity of the bound topological edge states I^- and I^+ provides a convenient way to excite them selectively. To this end, we employ a CPMD source that consists of two orthogonal magnetic dipole emitters with phase difference of $\pi/2$ ($-\pi/2$) to mimic the local pseudospin-down (pseudospin-up) source. We consider the case of a finite PhC with 23 periods as shown in Fig. 5(a), where the bound topological edge states become quasibound states with finite Q factors. CPMD sources with opposite spin states for excitation are placed at the cylinder marked in Fig. 5(a) and the finite-element method is used to evaluate the coupling between the CPMD sources and the quasibound topological edge states. The energy flux P_L (P_R) as a function of excitation frequency is calculated at the dashed line L (R) marked in Fig. 5(a) using a pseudospin-up (pseudospin-down) CPMD source and the normalized results are given in Figs. 5(b) and 5(c), from which one can see that edge states at the same frequency are successfully excited by the CPMD sources with opposite spin states. The electric field distributions at the peaks in Figs. 5(b) and 5(c) are shown in Figs. 5(d) and 5(e), respectively, where unidirectional excitation and propagation of the quasibound states can be clearly observed. We further calculate the directionality $D(x, y) = 2\,\mathrm{Im}(H_x^* H_y)/(|H_x|^2 + |H_y|^2)$ that is similar to the definition of Stokes parameter S_3 for guided modes [69] utilizing the eigenmode of I^+, where the result is given in Fig. 5(f). The corresponding normalized directionality $D(x, y) = (P_R - P_L)/(P_R + P_L)$ evaluated by the full-wave simulations using a pseudospin-up CPMD source at the same frequency of the eigensolution is shown in Fig. 5(g). As can be seen from Figs. 5(f) and 5(g), there is a decent agreement between the eigensolution and the full-wave simulation, indicating the possibility of manipulating the bound topological edge states by tuning the location of the CPMD source.

IV. EXPERIMENTAL DEMONSTRATIONS

In order to consolidate the theoretical results, we experimentally demonstrate the bound topological edge state in the continuum in the microwave region. The experimental setup used to validate the existence of quasibound topological edge states is shown in Fig. 6(a), where alumina ceramic pillars ($\varepsilon_r = 9.6$, $r = 8$ mm, $h = 11$ mm) are used to form the bulk PhC with $a = 80$ mm and the PhC is sandwiched between two aluminum plates to mimic the condition of a two-dimensional system (see also Fig. S3 within the Supplemental Material [68]). Homemade CPMD sources comprising two slightly detuned loop antennas orthogonal to each other [see the insets of Figs. 6(a)–6(c)] are connected to a vector network analyzer (VNA; R&S ZNB40) to irradiate microwaves at frequencies of around 1.9 GHz. As can be seen from the simulation and experimental results shown in Figs. 6(b) and 6(c), such antennas can produce electromagnetic near fields with Poynting vectors rotating in the clockwise and anticlockwise directions, respectively. An electric

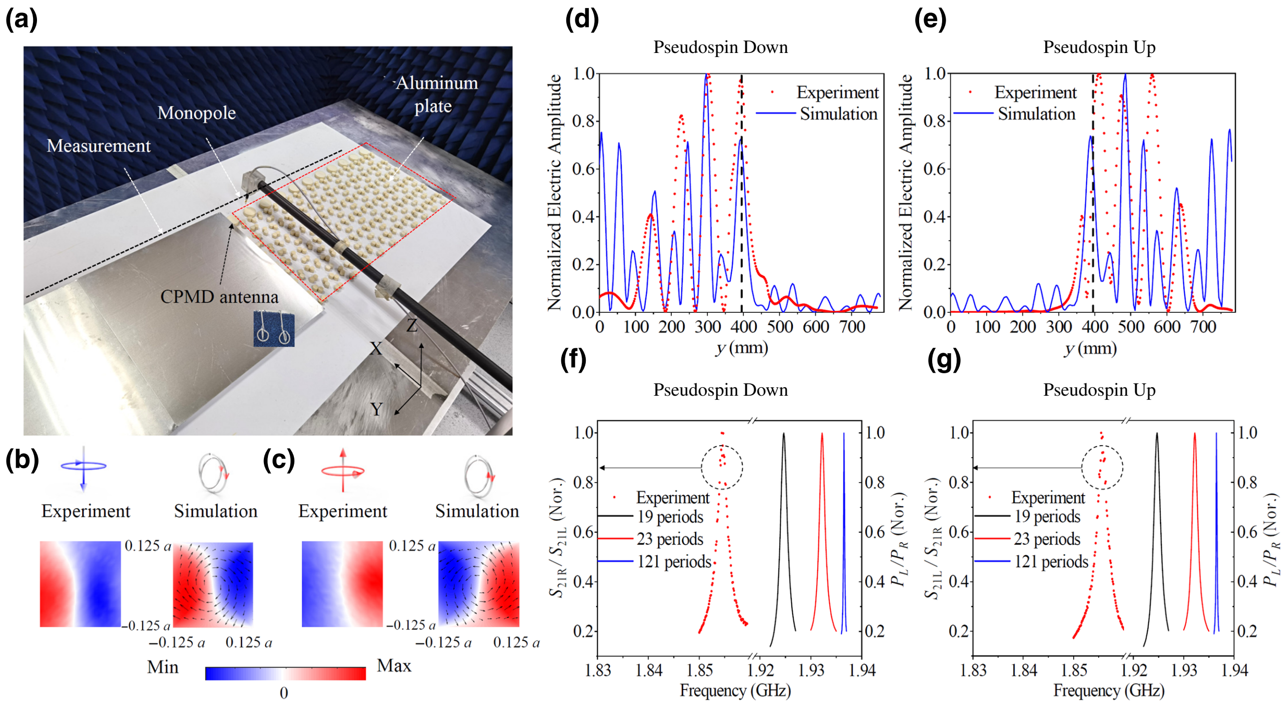

FIG. 6. (a) The experimental setup and the fabricated PhC. The PhC is sandwiched between two aluminum plates. A rectangular aluminum plate indicated by the red dashed rectangle is removed to visualize the PhC. Both the CPMD antennas and the electric monopole probe are shown by the insets. (b),(c) Schematics of pseudospin-down and pseudospin-up CPMD antennas, where the corresponding experimental and numerical results of electromagnetic near fields Re(E_z) are also presented. The Poynting vectors are indicated by the arrows. (d),(e) Experimental $|S_{21}|$ (red points) and simulated (blue solid lines) electric field amplitude ($|E_z|$) obtained at the black dashed line outlined in (a) under the excitation of pseudospin-down and pseudospin-up CPMD sources indicated by the vertical dashed line, respectively. (f),(g) The experimentally measured $S_{21R(L)}/S_{21L(R)}$ (red points) acquired at two points on the opposite sides of the CPMD sources, respectively. The corresponding simulated results $P_{R(L)}/P_{L(R)}$ (solid lines) for the PhC with larger periods are also given. All of them are normalized to their respective maxima.

monopole antenna connected to the VNA and mounted on a microwave scanning platform (LINBOU, NFS03 Floor Version) is used as an electric field probe to characterize the electric near field, which is acquired along a line close to the edge of the PhC, as indicated by the black dashed line in Fig. 6(a). Furthermore, microwave absorbers are used to minimize the impact of echo signals.

The measured S_{21} signal (red dots) of the electric monopole antenna proportional to the electric field component of E_z under the excitation of the pseudospin-down antenna at the frequency of quasibound topological edge states in the continuum is presented in Fig. 6(d), where the corresponding simulation result (solid blue line) is also provided for comparison (see also Figs. S4 and S5 within the Supplemental Material [68]). Although there is a discrepancy between the simulation and experimental results, which could be caused by the finite size effect of PEC claddings [see Fig. 6(a)], clear evidence of unidirectional excitation of the edge states by the CPMD antennas can be observed. The experimental measurement could be improved by using a scheme where the electric field on the inner surface of PEC claddings is acquired [18]. We further switch the source to the opposite spin state and perform the measurement at the same frequency. As can be seen from the results presented in Fig. 6(e), a reverse unidirectional propagating edge state is now excited at the same PhC. The normalized transmission spectra (red dots) for the states presented in Figs. 6(d) and 6(e) are shown in Figs. 6(f) and 6(g), respectively. It should be noted that compared with the simulation results (black lines) of the same size PhC, the Q factors obtained in the experiments (red dots) are smaller because of the non-negligible material absorption loss (see Fig. S6 within the Supplemental Material [68]). Moreover, there is a frequency shift between the simulation and experimental results, which may come from the difference of permittivity or size used in experiments and simulations. The Q factors of the edge states increase together with the increasing of the period number along the propagation direction, as shown in Figs. 6(f) and 6(g), indicating the BIC nature of these edge states (see also Fig. S5 within the Supplemental Material [68]). Finally, due to the topological nature of edge states, which originates from the nontrivial bulk topology of the frequency bands, these states could propagate against waveguide bends even though the operating frequency falls within the radiation continuum (see Fig. S7 within the Supplemental Material [68] for validation). Merging multiple BICs in momentum space can be used to enlarge the frequency range and increase the robustness of bound topological edge states in the continuum [58,64].

V. CONCLUSIONS AND OUTLOOK

In conclusion, we propose a physical mechanism to confine electromagnetic waves at the air edge of a topologically nontrivial PhC by exploiting the physics of BICs. These edge states exhibit topological features inherited from the nontrivial bulk band topology, which are further verified by microwave experiments. Our findings could shed light on topological photonics, where the bound topological edge state in the continuum could facilitate the reduction of footprint for topological devices, sensing [19,44], topological single-mode lasing [35,36], and high-harmonic generation using topological photonic modes above the light cone [70–72]. It is anticipated that our results might open an area of study where the nontrivial topology of bulk photonic bands can be exploited to enrich the physics of BICs. For instance, while we study the BIC physics in the context of the QSH effect, it is certainly interesting to see whether other members of the quantum Hall family, such as quantum Hall effect or quantum valley Hall effect, could be enlightened by the physics of BICs to facilitate more exotic phenomena.

ACKNOWLEDGMENTS

This research is supported by National Natural Science Foundation of China (NSFC) (Grants No. 91750110, No. 11674130, No. 61975177, and No. U20A20164), the Guangdong Introducing Innovative and Entrepreneurial Teams of "The Pearl River Talent Recruitment Program" (2019ZT08X340), and the Research and Development Plan in Key Areas of Guangdong Province (2018B010114002).

[1] M. Z. Hasan and C. L. Kane, Colloquium: Topological insulators, Rev. Mod. Phys. **82**, 3045 (2010).
[2] L. Lu, J. D. Joannopoulos, and M. Soljačić, Topological photonics, Nat. Photonics **8**, 821 (2014).
[3] T. Ozawa, H. M. Price, A. Amo, N. Goldman, M. Hafezi, L. Lu, M. C. Rechtsman, D. Schuster, J. Simon, O. Zilberberg, and I. Carusotto, Topological photonics, Rev. Mod. Phys. **91**, 015006 (2019).
[4] F. D. M. Haldane and S. Raghu, Possible Realization of Directional Optical Waveguides in Photonic Crystals with Broken Time-Reversal Symmetry, Phys. Rev. Lett. **100**, 013904 (2008).
[5] S. Raghu and F. D. M. Haldane, Analogs of quantum-hall-effect edge states in photonic crystals, Phys. Rev. A **78**, 033834 (2008).
[6] Z. Wang, Y. Chong, J. Joannopoulos, and M. Soljačić, Observation of unidirectional backscattering-immune topological electromagnetic states, Nature **461**, 772 (2009).
[7] Y. Poo, R. X. Wu, Z. F. Lin, Y. Yang, and C. T. Chan, Experimental Realization of Self-Guiding Unidirectional Electromagnetic Edge States, Phys. Rev. Lett. **106**, 093903 (2011).
[8] K. Fang, Z. Yu, and S. Fan, Realizing effective magnetic field for photons by controlling the phase of dynamic modulation, Nat. Photonics **6**, 782 (2012).
[9] M. C. Rechtsman, J. M. Zeuner, Y. Plotnik, Y. Lumer, D. Podolsky, F. Dreisow, S. Nolte, M. Segev, and A. Szameit, Photonic floquet topological insulators, Nature **496**, 196 (2013).
[10] M. Hafezi, S. Mittal, J. Fan, A. Migdall, and J. M. Taylor, Imaging topological edge states in silicon photonics, Nat. Photonics **7**, 1001 (2013).
[11] M. Hafezi, E. A. Demler, M. D. Lukin, and J. M. Taylor, Robust optical delay lines with topological protection, Nat. Phys. **7**, 907 (2011).
[12] A. B. Khanikaev, S. H. Mousavi, W.-K. Tse, M. Kargarian, A. H. MacDonald, and G. Shvets, Photonic topological insulators, Nat. Mater. **12**, 233 (2013).
[13] G. Q. Liang and Y. D. Chong, Optical Resonator Analog of a Two-Dimensional Topological Insulator, Phys. Rev. Lett. **110**, 203904 (2013).
[14] W. Chen, S. J. Jiang, X. D. Chen, B. Zhu, L. Zhou, J. W. Dong, and C. T. Chan, Experimental realization of photonic topological insulator in a uniaxial metacrystal waveguide, Nat. Commun. **5**, 5782 (2014).
[15] L. H. Wu and X. Hu, Scheme for Achieving a Topological Photonic Crystal by Using Dielectric Material, Phys. Rev. Lett. **114**, 223901 (2015).
[16] T. Ma, A. B. Khanikaev, S. H. Mousavi, and G. Shvets, Guiding Electromagnetic Waves around Sharp Corners: Topologically Protected Photonic Transport in Metawaveguides, Phys. Rev. Lett. **114**, 127401 (2015).
[17] C. He, X.-C. Sun, X.-P. Liu, M.-H. Lu, Y. Chen, L. Feng, and Y.-F. Chen, Photonic topological insulator with broken time-reversal symmetry, Proc. Natl. Acad. Sci. USA **113**, 4924 (2016).
[18] Y. Yang, Y. F. Xu, T. Xu, H. X. Wang, J. H. Jiang, X. Hu, and Z. H. Hang, Visualization of a Unidirectional Electromagnetic Waveguide Using Topological Photonic Crystals Made of Dielectric Materials, Phys. Rev. Lett. **120**, 217401 (2018).
[19] S. Barik, A. Karasahin, C. Flower, T. Cai, H. Miyake, W. DeGottardi, M. Hafezi, and E. Waks, A topological quantum optics interface, Science **359**, 666 (2018).
[20] W. Liu, Z. Ji, Y. Wang, G. Modi, M. Hwang, B. Zheng, V. J. Sorger, A. Pan, and R. Agarwal, Generation of helical topological exciton-polaritons, Science **370**, 600 (2020).
[21] M. L. N. Chen, L. J. Jiang, Z. Lan, and W. E. I. Sha, Pseudospin-polarized topological line defects in dielectric photonic crystals, IEEE Trans. Antennas Propag. **68**, 609 (2020).
[22] T. Ma and G. Shvets, All-Si valley-hall photonic topological insulator, New J. Phys. **18**, 025012 (2016).

[23] J. W. Dong, X. D. Chen, H. Zhu, Y. Wang, and X. Zhang, Valley photonic crystals for control of spin and topology, Nat. Mater. **16**, 298 (2017).

[24] X. D. Chen, F. L. Zhao, M. Chen, and J. W. Dong, Valley-contrasting physics in all-dielectric photonic crystals: Orbital angular momentum and topological propagation, Phys. Rev. B **96**, 020202(R) (2017).

[25] F. Gao, H. Xue, Z. Yang, K. Lai, Y. Yu, X. Lin, Y. Chong, G. Shvets, and B. Zhang, Topologically protected refraction of robust kink states in valley photonic crystals, Nat. Phys. **14**, 140 (2018).

[26] M. I. Shalaev, W. Walasik, A. Tsukernik, Y. Xu, and N. M. Litchinitser, Robust topologically protected transport in photonic crystals at telecommunication wavelengths, Nat. Nanotechnol. **14**, 31 (2019).

[27] X. T. He, E. T. Liang, J. J. Yuan, H. Y. Qiu, X. D. Chen, F. L. Zhao, and J. W. Dong, A silicon-on-insulator slab for topological valley transport, Nat. Commun. **10**, 872 (2019).

[28] M. L. N. Chen, L. J. Jiang, Z. Lan, and W. E. I. Sha, Coexistence of pseudospin- and valley-hall-like edge states in a photonic crystal with C_3v symmetry, Phys. Rev. Res. **2**, 043148 (2020).

[29] W. Gao, M. Lawrence, B. Yang, F. Liu, F. Fang, B. Béri, J. Li, and S. Zhang, Topological Photonic Phase in Chiral Hyperbolic Metamaterials, Phys. Rev. Lett. **114**, 037402 (2015).

[30] L. Lu, C. Fang, L. Fu, S. G. Johnson, J. D. Joannopoulos, and M. Soljačić, Symmetry-protected topological photonic crystal in three dimensions, Nat. Phys. **12**, 337 (2016).

[31] Y. Yang, Z. Gao, H. Xue, L. Zhang, M. He, Z. Yang, R. Singh, Y. Chong, B. Zhang, and H. Chen, Realization of a three-dimensional photonic topological insulator, Nature **565**, 622 (2019).

[32] H. Zhou, C. Peng, Y. Yoon, C. W. Hsu, K. A. Nelson, L. Fu, J. D. Joannopoulos, M. Soljačić, and B. Zhen, Observation of bulk fermi arc and polarization half charge from paired exceptional points, Science **359**, 1009 (2018).

[33] B. Yang, Q. Guo, B. Tremain, R. Liu, L. E. Barr, Q. Yan, W. Gao, H. Liu, Y. Xiang, J. Chen, C. Fang, A. Hibbins, L. Lu, and S. Zhang, Ideal Weyl points and helicoid surface states in artificial photonic crystal structures, Science **359**, 1013 (2018).

[34] X. Gao, L. Yang, H. Lin, L. Zhang, J. Li, F. Bo, Z. Wang, and L. Lu, Dirac-vortex topological cavities, Nat. Nanotechnol. **15**, 1012 (2020).

[35] G. Harari, M. A. Bandres, Y. Lumer, M. C. Rechtsman, Y. D. Chong, M. Khajavikhan, D. N. Christodoulides, and M. Segev, Topological insulator laser: Theory, Science **359**, eaar4003 (2018).

[36] M. A. Bandres, S. Wittek, G. Harari, M. Parto, J. Ren, M. Segev, D. N. Christodoulides, and M. Khajavikhan, Topological insulator laser: Experiments, Science **359**, eaar4005 (2018).

[37] Z. K. Shao, H. Z. Chen, S. Wang, X. R. Mao, Z. Q. Yang, S. L. Wang, X. X. Wang, X. Hu, and R. M. Ma, A high-performance topological bulk laser based on band-inversion-induced reflection, Nat. Nanotechnol. **15**, 67 (2020).

[38] Z. Q. Yang, Z. K. Shao, H. Z. Chen, X. R. Mao, and R. M. Ma, Spin Momentum-Locked Edge Mode for Topological Vortex Lasing, Phys. Rev. Lett. **125**, 013903 (2020).

[39] J. Noh, W. A. Benalcazar, S. Huang, M. J. Collins, K. P. Chen, T. L. Hughes, and M. C. Rechtsma, Topological protection of photonic mid-gap defect modes, Nat. Photonics **12**, 408 (2018).

[40] Y. Wang, W. Liu, Z. Ji, G. Modi, M. Hwang, and R. Agarwal, Coherent interactions in one-dimensional topological photonic systems and their applications in all-optical logic operation, Nano Lett. **20**, 8796 (2020).

[41] J. von Neumann and E. Wigner, Über merkwürdige diskrete eigenwerte, Phys. Z. **30**, 465 (1929).

[42] C. W. Hsu, B. Zhen, A. D. Stone, J. D. Joannopoulos, and M. Soljačić, Bound states in the continuum, Nat. Rev. Mater. **1**, 16048 (2016).

[43] E. N. Bulgakov and A. F. Sadreev, Bound states in the continuum in photonic waveguides inspired by defects, Phys. Rev. B **78**, 075105 (2008).

[44] D. C. Marinica, A. G. Borisov, and S. V. Shabanov, Bound States in the Continuum in Photonics, Phys. Rev. Lett. **100**, 183902 (2008).

[45] R. F. Ndangali and S. V. Shabanov, Electromagnetic bound states in the radiation continuum for periodic double arrays of subwavelength dielectric cylinders, J. Math. Phys. (N.Y.) **51**, 102901 (2010).

[46] Y. Plotnik, O. Peleg, F. Dreisow, M. Heinrich, S. Nolte, A. Szameit, and M. Segev, Experimental Observation of Optical Bound States in The Continuum, Phys. Rev. Lett. **107**, 183901 (2011).

[47] F. Monticone and A. Alù, Embedded Photonic Eigenvalues in 3D Nanostructures, Phys. Rev. Lett. **112**, 213903 (2014).

[48] J. Lee, B. Zhen, S.-L. Chua, W. Qiu, J. D. Joannopoulos, M. Soljačić, and O. Shapira, Observation and Differentiation of Unique High-Q Optical Resonances Near Zero Wave Vector in Macroscopic Photonic Crystal Slabs, Phys. Rev. Lett. **109**, 067401 (2012).

[49] C. W. Hsu, B. Zhen, J. Lee, S. L. Chua, S. G. Johnson, J. D. Joannopoulos, and M. Soljačić, Observation of trapped light within the radiation continuum, Nature **499**, 188 (2013).

[50] B. Zhen, C. W. Hsu, L. Lu, A. D. Stone, and M. Soljačić, Topological Nature of Optical Bound States in the Continuum, Phys. Rev. Lett. **113**, 257401 (2014).

[51] Y. Yang, C. Peng, Y. Liang, Z. Li, and S. Noda, Analytical Perspective for Bound States in the Continuum in Photonic Crystal Slabs, Phys. Rev. Lett. **113**, 037401 (2014).

[52] Y. Zhang, A. Chen, W. Liu, C. W. Hsu, B. Wang, F. Guan, X. Liu, L. Shi, L. Lu, and J. Zi, Observation of Polarization Vortices in Momentum Space, Phys. Rev. Lett. **120**, 186103 (2018).

[53] H. M. Doeleman, F. Monticone, W. den Hollander, A. Alù, and A. F. Koenderink, Experimental observation of a polarization vortex at an optical bound state in the continuum, Nat. Photonics **12**, 397 (2018).

[54] M. Minkov, I. A. D. Williamson, M. Xiao, and S. Fan, Zero-Index Bound States in the Continuum, Phys. Rev. Lett. **121**, 263901 (2018).

[55] K. Koshelev, S. Lepeshov, M. Liu, A. Bogdanov, and Y. Kivshar, Asymmetric Metasurfaces with High-Q Resonances Governed by Bound States in the Continuum, Phys. Rev. Lett. **121**, 193903 (2018).

[56] A. Tittl, A. Leitis, M. Liu, F. Yesilkoy, D. Y. Choi, D. N. Neshev, Y. S. Kivshar, and H. Altug, Imaging-based molecular barcoding with pixelated dielectric metasurfaces, Science **360**, 1105 (2018).

[57] Z. Liu, Y. Xu, Y. Lin, J. Xiang, T. Feng, Q. Cao, J. Li, S. Lan, and J. Liu, High-Q Quasibound States in the Continuum for Nonlinear Metasurfaces, Phys. Rev. Lett. **123**, 253901 (2019).

[58] J. Jin, X. Yin, L. Ni, M. Soljačić, B. Zhen, and C. Peng, Topologically enabled ultra-high-Q guided resonances robust to out-of-plane scattering, Nature **574**, 501 (2019).

[59] W. Liu, B. Wang, Y. Zhang, J. Wang, M. Zhao, F. Guan, X. Liu, L. Shi, and J. Zi, Circularly Polarized States Spawning from Bound States in the Continuum, Phys. Rev. Lett. **123**, 116104 (2019).

[60] X. Yin, J. Jin, M. Soljačić, C. Peng, and B. Zhen, Observation of unidirectional bound states in the continuum enabled by topological defects, Nature **580**, 467 (2020).

[61] B. Wang, W. Liu, M. Zhao, J. Wang, Y. Zhang, A. Chen, F. Guan, X. Liu, L. Shi, and J. Zi, Generating optical vortex beams by momentum-space polarization vortices centred at bound states in the continuum, Nat. Photonics **14**, 623 (2020).

[62] C. Huang, C. Zhang, S. Xiao, Y. Wang, Y. Fan, Y. Liu, N. Zhang, G. Qu, H. Ji, J. Han, L. Ge, Y. Kivshar, and Q. Song, Ultrafast control of vortex microlasers, Science **367**, 1018 (2020).

[63] Y. Lin, T. Feng, S. Lan, J. Liu, and Y. Xu, On-Chip Diffraction-Free Beam Guiding Beyond the Light Cone, Phys. Rev. Appl. **13**, 064032 (2020).

[64] M. Kang, S. Zhang, M. Xiao, and H. Xu, Merging Bound States in the Continuum at Off-High Symmetry Points, Phys. Rev. Lett. **126**, 117402 (2021).

[65] M. I. Molina, A. E. Miroshnichenko, and Y. S. Kivshar, Surface Bound States in the Continuum, Phys. Rev. Lett. **108**, 070401 (2012).

[66] S. Weimann, Y. Xu, R. Keil, A. E. Miroshnichenko, A. Tünnermann, S. Nolte, A. A. Sukhorukov, A. Szameit, and Y. S. Kivshar, Compact Surface Fano States Embedded in the Continuum of Waveguide Arrays, Phys. Rev. Lett. **111**, 240403 (2013).

[67] C. W. Hsu, B. Zhen, S.-L. Chua, S. G. Johnson, J. D. Joannopoulos, and M. Soljačić, Bloch surface eigenstates within the radiation continuum, Light Sci. Appl. **2**, e84 (2013).

[68] See Supplemental Material at http://link.aps.org/supplemental/10.1103/PhysRevApplied.16.064036 for dispersion and Q factors of eigenmodes for infinite structures, PhC structures used in the microwave experiment, additional simulation results for finite structures, verification of the BIC, and verification of the topological nature of the edge state.

[69] M. Born and E. Wolf, *Principle of Optics* (Cambridge University Press, Cambridge, UK, 1999), p. 31.

[70] D. Smirnova, S. Kruk, D. Leykam, E.M. Gaykazyan, D.-Y. Choi, and Y. Kivshar, Third-Harmonic Generation in Photonic Topological Metasurfaces, Phys. Rev. Lett. **123**, 103901 (2019).

[71] S. S. Kruk, W. Gao, D. Choi, T. Zentgraf, S. Zhang, and Y. Kivshar, Nonlinear imaging of nanoscale topological corner states, Nano Lett. **21**, 4592 (2021).

[72] J. Wang, M. Clementi, M. Minkov, A. Barone, J. Carlin, N. Grandjean, D. Gerace, S. Fan, M. Galli, and R. Houdré, Doubly resonant second-harmonic generation of a vortex beam from a bound state in the continuum, Optica **7**, 1126 (2020).